The American Journal of Pathology, Vol. 195, No. 9, September 2025

The American Journal of
PATHOLOGY
ajp.amjpathol.org

MACHINE LEARNING, COMPUTATIONAL PATHOLOGY, AND BIOPHYSICAL IMAGING

Super-Resolution Microscopy Reveals Alterations in Clathrin Structure in Human Cancer Tissue

Alan Greig,[*] Rui Henrique,[†] Boyu Xie,[‡] Christopher Thrasivoulou,[*] Michael Millar,[§] and Aamir Ahmed[*‡]

From Cell and Developmental Biology,[*] University College London, London, United Kingdom; the Department of Pathology and Cancer Biology and Epigenetics Group,[†] Portuguese Oncology Institute of Porto and Porto Comprehensive Cancer Center Raquel Seruca (Porto CCC) and Department of Pathology and Molecular Immunology, School of Medicine and Biomedical Sciences, University of Porto, Porto, Portugal; the Centre for Stem Cells and Regenerative Medicine,[‡] King's College London, London, United Kingdom; and the Institute for Regeneration and Repair,[§] University of Edinburgh, Edinburgh, United Kingdom

Accepted for publication May 20, 2025.

Address correspondence to Aamir Ahmed, Ph.D., Cell and Developmental Biology, University College London, Rockefeller Building, London WC1E 6DE, United Kingdom. E-mail: aamir.ahmed@ucl.ac.uk.

Super-resolution microscopy holds great promise for detailed structural analysis of proteins, yet its application in the investigations of protein structures *in situ* remains sparse. Clathrin-coated pit-mediated endocytosis (CME) plays a key role in human cancer. This study aimed to discover whether there are structural changes in clathrin pits in cancer. Immunofluorescence combined with super-resolution structured illumination microscopy (SR-SIM) on normal and cancerous prostate tissue was used to reveal novel details of clathrin structure and biology. Clathrin (heavy-chain) plaques and pits, expression of adaptor protein 2 (a clathrin adaptor protein), and epidermal growth factor receptor (a receptor target for CME) at nanometer scale in human tissue were observed *in situ* with immunofluorescence-SR-SIM. The size of the clathrin pits in high-grade cancer was greater compared with that in low-grade or normal prostate tissue. These results demonstrate that SR-SIM can be used to identify protein structures at high resolution in clinical tissue sections and there is an increased cargo capacity due to the increase in the size of clathrin pits as a mechanism that facilitates aggressiveness of cancer. These results shed new light on the pathology of cancer and the role CME via clathrin may play in carcinogenesis. *(Am J Pathol 2025, 195: 1619–1626; https://doi.org/10.1016/j.ajpath.2025.05.008)*

Clathrin, comprising of heavy (180 to 190 kDa) and light (25 kDa) chains, is a scaffold protein that forms a triskelion structure.[1] Clathrins form coated vesicles for exocytosis and endocytosis in cells and material transport across the plasma membrane by forming honeycomb lattice on the cytoplasmic surface of coated pits. The clathrin pits are largely seen on the plasma membrane but also occur in the trans-Golgi network. Clathrin complex formation also requires adaptors, such as the adaptor protein (AP1-5) family. For example, AP1 is essential for clathrin-coated vesicles at the trans-Golgi network, whereas AP2 is involved at the pinching site on the plasma membrane.[2] These elements along with phosphatidylinositol-4,5-bisphosphate are essential for clathrin pit-mediated endocytosis (CME), a disposal and recycling system in mammalian cells.[3] A key function of CME is the likely recycling of membrane signaling receptor proteins.

Clathrin pit formation involves the assembly of clathrin-coated vesicles into a curved clathrin lattice (eg, containing cargo, such as membrane receptors), which is linked through adaptor proteins (eg, AP2) on the cell surface.[4] Increased availability of receptors, such as those for epidermal growth factor receptor (EGFR) or Wnt signaling, may have a direct consequence on cell proliferation. Immunofluorescence microscopy shows that clathrin expression is up-regulated in prostate cancer tissue and that expression of clathrin progressively increased with cancer aggressiveness in conjunction with increased colocalization of EGFR receptor.[5] There is an increased recycling of EGFR as carcinogenesis progresses, although how this

Supported by the Prostate Cancer Research Centre number AA1 and King's College Development Fund.

Copyright © 2025 American Society for Investigative Pathology. Published by Elsevier Inc.
This is an open access article under the CC BY-NC-ND license (*http://creativecommons.org/licenses/by-nc-nd/4.0*).
https://doi.org/10.1016/j.ajpath.2025.05.008

increased recycling may occur is not known. The shift from EGFR from degradation to recycling can play a significant role in the pathology of cancer.

The structure of clathrin has been extensively investigated in model cellular systems, such as cancer cell lines, using optical and electron microscopy (EM). However, little is known about structural changes that may occur during disease in human tissue. Such investigations are essential for the understanding of structure and microdistribution of clathrin and how it may be modulated during the pathogenesis of cancer, with critical functional consequences. This lack of structural insight, particularly in human tissue, is most likely due to accessibility of human tissue and highly specialized nature of EM. Although EM can achieve resolution at subnanometer scale, the laborious nature of sample preparation, limited application in a large number of samples, technical knowhow, and limited accessibility are major impediments in its use as a common microscopic technique for the investigations of ultrastructure of proteins,[6] particularly in human tissue sections. Combining super-resolution structured illumination microscopy (SR-SIM) with commonly used immunofluorescence can help elucidate three-dimensional structural details of proteins, such as clathrin, to delineate their function and regulation.[7]

SR-SIM can also achieve resolution at the nanometer scale, that allows structural detail that is usually only achievable with EM.[8,9] As SR microscopy becomes more accessible,[6] SR-SIM can provide a more amenable and convenient method of investigating structural characterization of proteins, as compared to that with EM. SR-SIM is also advantageous over other super-resolution microscopy methods because it retains some ability to resolve objects smaller than the diffraction limit even in thicker samples, such as tissue sections. Combining SR-SIM with immunochemistry adds a layer of validation and detail for the structural investigations of proteins and their role in the pathology of epithelial cancers.

We hypothesize that there is an increase in the size of clathrin-coated pits in aggressive cancer tissue compared with that in low-grade prostate cancer tissue. This could provide a mechanism allowing an increase in the cargo carried by clathrin-coated vesicles. To test this hypothesis, a combination of SR-SIM and immunofluorescence was used to characterize the structure of clathrin in normal and cancerous human prostate tissue. SR-SIM was capable of resolving clathrin pits of diameter less than the diffraction limit in human tissue sections. Thus, an analysis of the super-resolution images can be used to investigate key mechanisms of carcinogenesis.

Materials and Methods

TA Construction and Immunohistochemistry

Ethical approval was granted by the joint research office of University College London and University College Hospital through East of Scotland Research Ethics Service (REC reference 13/ES/0092). Samples, described as cancer or normal and of different stages of cancer, were diagnosed before and after tissue array (TA) construction by an expert pathologist (R.H.).

TAs used in this study have been described in detail elsewhere.[5] Tissue from 15 patients was used to make tissue arrays with 60 individual cores from cancer area and paired cancer-adjacent normal area, as described previously.[5] TAs were sectioned (using a HM355S automatic microtome; Thermo Fisher Scientific, Waltham, MA) and stained with hematoxylin and eosin for histologic examination or with anti-clathrin (heavy chain; ab21679; Abcam, Cambridge, UK; 1:2000 labeled with Opal 650), AP2 (ab2910; Abcam; 1:500; Opal 520), and EGFR (NCL-EGFR; Leica Biosystems, Sheffield, UK; 1:20; Opal 570) antibodies for protein expression and structural analysis, as described previously.[5] An extensive optimization procedure (eg, pH and concentration dependence, antigen retrieval, and temperature dependency) was used on whole prostate tissue sections before the use of antibodies on TA sections.[5] Multiplex staining of TAs is an established protocol in the laboratory[10,11] using the Bond RX automated staining system (Leica Biosystems).

TA Imaging Using Fluorescence and Confocal Microscopy

This has been previously described in detail.[5] Briefly, an overview of the labeled TAs was obtained using AxioScan Z1 scanner (Carl Zeiss, Jena, Germany) at $\times$20 magnification. To obtain higher-resolution images of clathrin, AP2, and EGFR expression, confocal imaging was performed using a Leica SP8 microscope (Leica Microsystems, Wetzlar, Germany).[5] Confocal images thus obtained were deconvolved using Huygens Professional software version 23.10 (SVI, Hilversum, the Netherlands).

Super-Resolution Imaging of Human Prostate Tissue

Cancer and normal tissue samples on two tissue array slides were imaged using a super-resolution ELYRA 7 (Zeiss) lattice structured illumination microscope (Lattice SIM). Various internal and quality controls were established and care was taken to avoid any known artefacts, as described in Supplemental Figure S1 and the text below. The optical resolution of the microscope was verified by quantifying the dimensions of TetraSpek nanobeads (Thermo Fisher Scientific) as recommended by the manufacturer and by assessment of both the illumination lattice in the raw images and the SIM^2 reconstruction of the processed images in Fourier space (Supplemental Figure S1).

The ELYRA 7 system in SIM mode uses five mutually coherent light beams to generate an interference pattern, which forms a lattice when projected through an objective lens. The lattice pattern provides isotropic resolution improvement in all three dimensions.[12] The lattice structure

itself was shifted laterally in 15 phases to generate Moiré fringes. Images were acquired using a 63×, 1.46 numerical aperture objective lens, and excitation was achieved with 488-, 561-, and 638-nm laser lines for AP2, EGFR, and clathrin heavy chain, respectively. Collected images were processed using ZenBlack 3.0 SR SIM^2 software (Zeiss).

TAs were sectioned at 6 μm to minimize any systematic difference in z-position across the samples; the first imaged z-slice was always collected within 1 μm from the surface of the section, ensuring that there was little or no z-aberration differences when comparing across samples. As a fluorescence super-resolution microscopy approach was used, the images were collected in a manner that maximized the signal yield and prevented bleaching of the specimen. Also, quality control was conducted to eliminate artefacts and determine the robustness of the technique as follows: First, the signal-to-noise ratio (SNR) of the raw images was calculated by using the minimum and maximum function on the display tab in ZenBlack software. The median SNR was calculated to be 7.6 ± 3.5 fold (median ± SD; 95% CI for the median = 6.0−9.6; $N = 8$; $n = 28$) using the minimum and maximum values on the distribution histogram using ZenBlack software; the SNR was considered high enough[13] to permit selection of strong (high) SNR in the SIM^2 processing tab in ZenBlack software. This also informed setting the number of iterations to 25 and the regularization weight to 0.007 automatically, and it is these values that are termed strong for SIM^2 processing (ZenBlack software). The SIM^2 processing parameters were kept constant across all Z-stacks processed and displayed in this study. Furthermore, an assessment of quality of the SIM^2 processed and unprocessed images (Supplemental Figure S1) was made to ensure that the lattice was visible in the unprocessed images and not in the SIM^2 processed images.

For this study normal, Gleason grades 3 + 3, 4 + 4, and 4 + 5 were imaged using the ELYRA 7 microscope. As this is a first report of the use of super-resolution microscopy to analyze clathrin structure, the number of images to be analyzed was oversampled. Thus, a total of 254 images were accrued from two tissue array slides representing 15 individual patients covering four different diagnoses: normal (cancer adjacent) and Gleason grades 3 + 3, 4 + 4, and 4 + 5. The following samples from TA were imaged for super-resolution analysis: normal ($n = 76$); 3 + 3 ($n = 60$); 4 + 4 ($n = 47$); and 4 + 5 ($n = 71$).

Data Acquisition and Analysis

The SR SIM^2 images were used to investigate the detailed structural analysis of clathrin using the ZenBlack image analysis software. Images were cropped to allow identification and measurement of individual clathrin pits, and the line profile measurement tool was used to measure the diameter of each pit. As this is a first such investigation of clathrin pits using super-resolution microscopy, between 5 and 24 such measurements were made from each tissue core so as not to undersample the number of individual measurements. Making such measurements from individual tissue cores was also important to oversample because any putative biological difference needed to have a robust underpinning. Care was taken to use as many clathrin pits as possible where AP2 expression was correlated. Quantification of the intensity signal for clathrin expression in SIM^2 processed images was conducted using the maximum projection tool histogram widget in ZenBlack software. The diameters thus measured were used to calculate the clathrin pit size and any differences in normal and cancer or within different grades of prostate cancer. Statistical analysis was performed using MedCalc (MedCalc Software Ltd., Ostend, Belgium).

Results

TAs with tissue samples from cancer and normal human prostate tissue were used for this study.[5] The tissue array was previously probed with clathrin, AP2, and EGFR antibodies.[5] Representative low-magnification (×20), fluorescence image (Figure 1, A and B for cancer and normal tissue, respectively) and high-magnification (×63) deconvolved confocal image (Figure 1, C and D) are shown. For this study, TAs were imaged using lattice structured illumination on an ELYRA 7 (Carl Zeiss) super-resolution microscope, using a 63× lens with a numerical aperture of 1.46, which gave a pixel size of 0.02 μm^2 following SIM^2 processing.

The raw images with the fluorophore signal for the heavy chain of clathrin, AP2, and EGFR are shown in Supplemental Figure S2 for cancer adjacent normal and cancerous tissue, respectively. These images were processed using the ELYRA 7's SIM^2 tools for further analysis. First, the expression and structure of clathrin in the SIM^2 processed images were investigated (Figure 2). A z-series of images exhibit a lattice structure in which clathrin plaques (Figure 2A) can be seen. Several clathrin triskelion structures (Figure 2, B−D) were visible across these sequential images (Supplemental Video S1 of the z-series). These results indicate that clathrin in the form of plaques and pits can be identified using super-resolution microscopy. These images further suggested that the ultrastructure of clathrin can be investigated, in large numbers of human tissue samples with medium analytical throughput.

To confirm that the structures observed in Figure 2 were clathrin pits, the expression of clathrin with its associated protein AP2 and the EGFR receptor protein, likely to be expressed in the cell membrane, was investigated. The expression of clathrin, AP2, and EGFR could be observed in SIM^2 processed, low-magnification composite images (Figure 3, A and G, for normal and cancerous prostate tissue sample, respectively). The clathrin expression in the form of pits was more discernible with intermediate digital magnification (Figure 3, B and H, for normal and cancer, respectively). Further digitally zoomed composite images

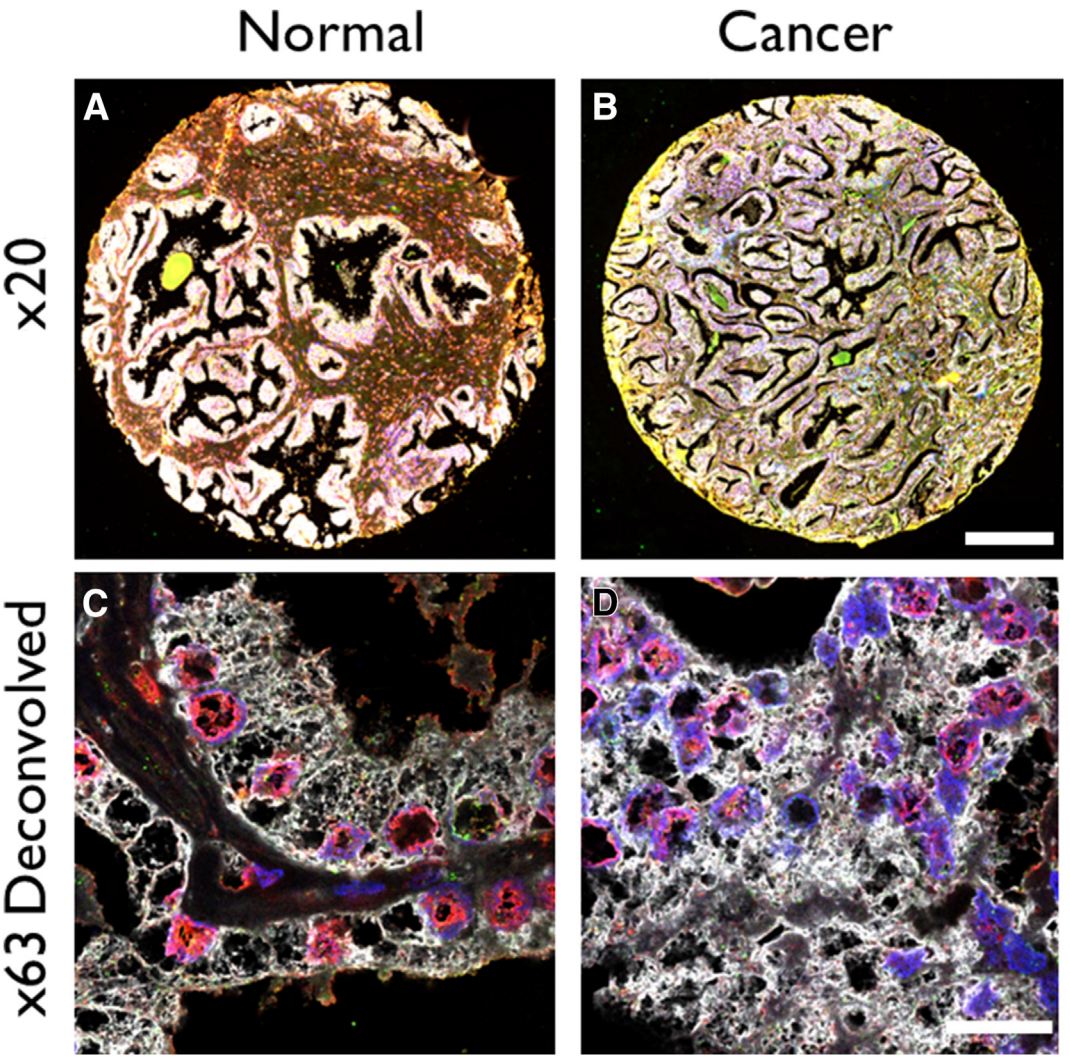

Figure 1 Representative images of cancer and normal human prostate tissue probed for clathrin heavy chain (white), adaptor protein 2 (red), epidermal growth factor receptor (green), and DAPI nuclear stain (blue) using fluorescence microscopy [normal (**A**) and cancer (**B**) tissue core, respectively], deconvolved confocal microscopy images [normal (**C**) and cancer (**D**) tissue, respectively]. These images are shown for illustrative purposes only and as examples of the source material for super-resolution microscopy. The tissue samples, such as the one shown in **A** and **B**, were used for microscopy using ELYRA 7 super-resolution microscope. Scale bars: 200 μm (**A** and **B**); 18 μm (**C** and **D**). Original magnifications: ×20 (**A** and **B**); ×63 (**C** and **D**).

(Figure 3, C and I, for normal and cancer, respectively) clearly showed clathrin pits associated with AP2 and EGFR proteins with the triskelion structure, characteristic of clathrin pits (Figure 3, D–F and J–L, are single-fluorophore source images used for the construction of composite images). A three-dimensional rendering, with schematic representation, of a clathrin pit, with a cup-like structure, with associated AP2 and EGFR proteins is given in Supplemental Figure S3.

Clathrin expression is increased in cancerous prostate tissue compared with normal prostate, as indicated by confocal imaging.[5] A semiquantitative analysis of clathrin signal intensity confirmed these observations (Figure 4A). There was a significant increase in the expression of clathrin in all Gleason grades of prostate cancer investigated compared with that in normal tissue. There was also a progressive increase in the expression of clathrin in different Gleason grades, except in the comparison between Gleason grade 3 + 3 and 4 + 4 (Figure 4A).

An increase in the clathrin expression is indicative of its critical role in CME and in carcinogenesis (Figure 4A).[5] What is not clear is whether there is also modulation in the size of the clathrin pits in prostate cancer, particularly in different pathologic grades of prostate cancer. Therefore, measurements were made of clathrin pits using the line profile measurement tool in the ZenBlack software from the SIM^2 processed images of human prostate tissue.

A total of 254 individual image frames were analyzed across four different conditions (normal, prostate cancer tissue of Gleason grades 3 + 3, 4 + 4, and 4 + 5, initially characterized by an expert pathologist). The median pit diameter (μm) ranged between 0.10 (low, 0.05; and high, 0.23; with 95% CI of 0.09–0.11) for normal prostate tissue, to 0.12 (low, 0.06; and high, 0.22; with 95% CI of

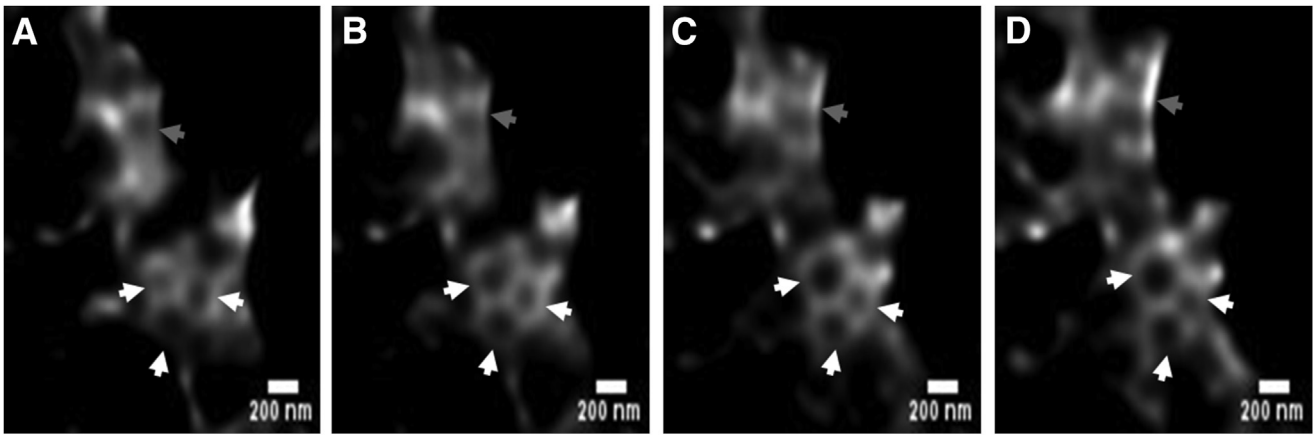

Figure 2 Clathrin pits and a honeycomb lattice visible across a segment of human prostate tissue section using the ELYRA 7 super-resolution structured illumination microscopy (SIM) system. The honeycomb is made up of polyhedral structures, pentagons, and hexagons that represent the assembly of the characteristic triskelions (also see Supplemental Video S1). **A**–**D:** Axial data set of x, y images through area of clathrin-positive prostate tissue subsequent to SIM^2 processing. Two known conformations of clathrin are apparent within the images, clathrin plaques (**gray arrows**) and clathrin pit structures (**white arrows**). Both conformations are present in our data sets, and the images presented here are representative. The x-, y-, and z-scaling were set at 16, 16, and101 nm, respectively. Scale bar = 200 nm (**A**–**D**).

0.11–0.13), 0.12 (low, 0.06; and high, 0.18; with 95% CI of 0.11–0.12), and 0.16 (low, 0.05; and high, 0.27; with 95% CI of 0.15–0.17) for Gleason grades 3 + 3, 4 + 4, and 4 + 5, respectively. These measured pit diameters compared well with the published data on the clathrin pit size derived largely through electron microscopy.[14] A distribution histogram of the clathrin pit with a comparison between normal and different Gleason grades is shown in Supplemental

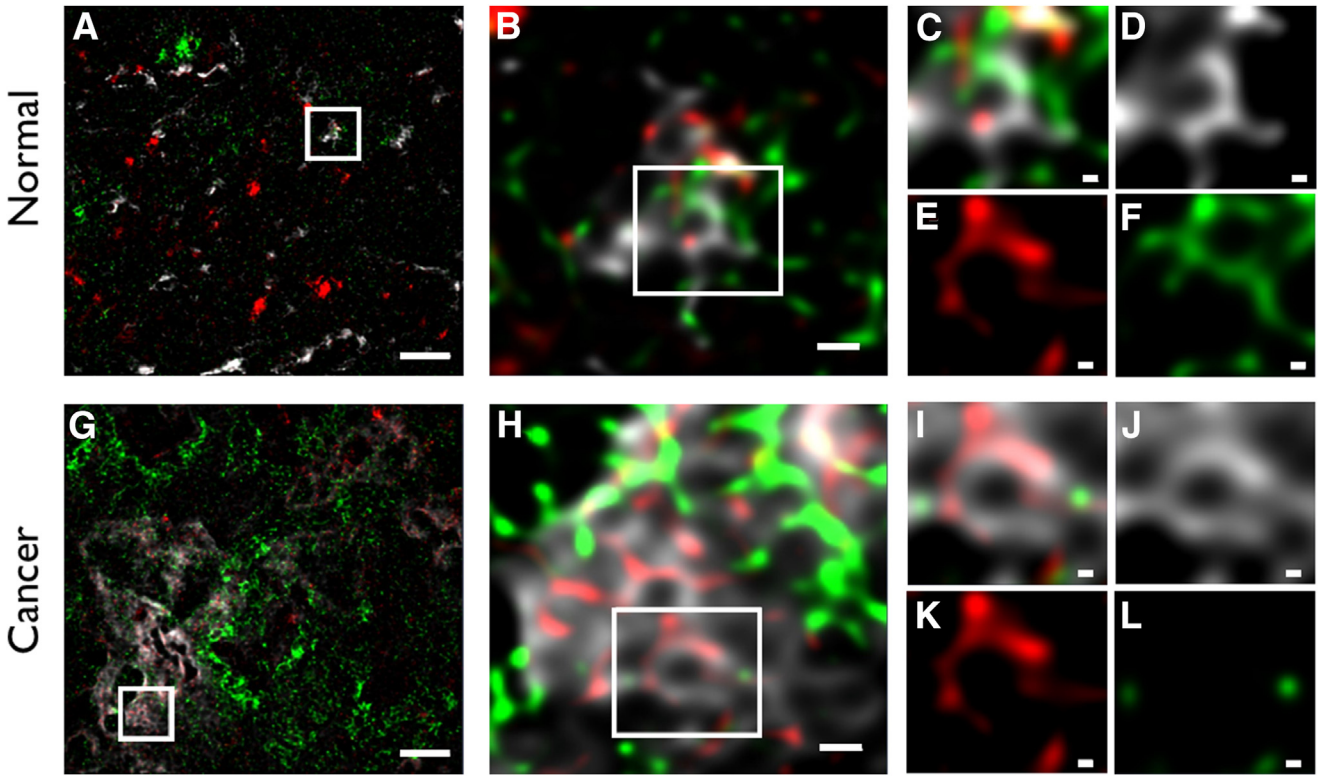

Figure 3 Representative single-slice composite of clathrin heavy chain (white), adaptor protein AP2 (red), and epidermal growth factor receptor (green) in human prostate tissue. **A**–**L:** An original structured illumination microscopy SIM^2 processed Z-stack [cancer adjacent normal (**A**) and cancer (**G**) prostate tissue sections, respectively] showing a broad field of view and subsequently (**white boxed areas**) with digital zoom of increasing magnifications showing an intermediate field (**B** and **H**) and zoomed-in field (**C**–**F** and **I**–**L**). **D**–**F** and **J**–**L:** Zoomed-in single-fluorophore images from which the zoomed-in composite images **C** and **I**, respectively, were constructed. Scale bars: 2 μm (**A** and **G**); 0.2 μm (**B** and **H**); 0.05 μm (**C**–**F** and **I**–**L**).

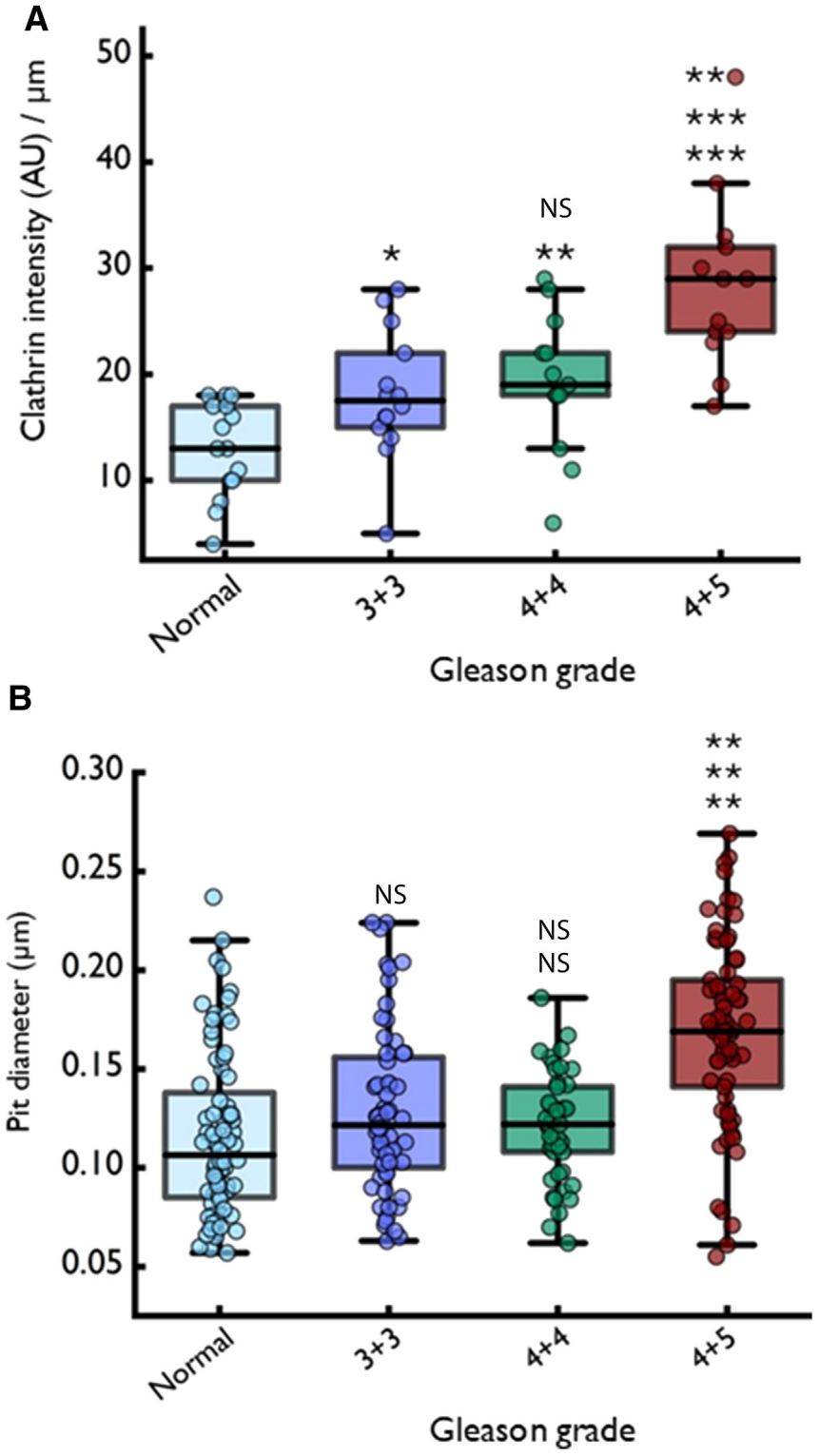

Figure 4 **A:** Semiquantitative analysis of clathrin expression calculated as pixel intensity/area (µm) from a sampled cohort. Images from an ELYRA 7 (Zeiss) microscope were processed using the structured illumination microscopy SIM^2 method and analyzed for clathrin signal using ZenBlack (Zeiss) intensity measurement tool for normal, and Gleason grade 3 + 3, 4 + 4, and 4 + 5 prostate tissue. There was a significant increase in the expression of clathrin in different cancer grades compared with cancer adjacent normal tissue (*U*-test); there was also a significant increase in the expression of clathrin in high-grade (4 + 5) prostate cancer compared with Gleason grades 3 + 3 or 4 + 4; no significant difference between low grades 3 + 3 and 4 + 4 graded prostate cancer. **B:** A box plot of pit size diameters for normal, and cancer grades 3 + 3, 4 + 4, and 4 + 5 prostate tissue. There was no significant change in the pit size in cancer grade 3 + 3 or 4 + 4 when compared with normal prostate. There was a significant ($P < 0.01$) increase in the pit diameter in cancer grade 4 + 5 compared with all other conditions (*U*-test). $n = 13$ to 15 (**A**). *$P < 0.05$, **$P < 0.01$, and ***$P < 0.001$. AU, arbitrary unit; NS, nonsignificant.

Figure S4. An overall distribution for all samples is given in Supplemental Figure S4A, followed by normal versus Gleason grade (Supplemental Figure S4, B–D) and between Gleason grades (Supplemental Figure S4, E–G). The pit diameter distribution only showed a shift to the right of the histogram when comparisons are made with high Gleason grade (4 + 5) tissue samples. This observation was further validated on significance testing (Figure 4B) where the only significant differences measured were between normal or Gleason grades 3 + 3 and 4 + 4 versus Gleason grade 4 + 5 samples. These results indicate that in addition to an increase in the expression of clathrin in high Gleason grade prostate cancer, there is also an increase in the clathrin pit diameter (Figure 4B).

Discussion

CME and the structure of clathrin has a long history of investigation in model cellular systems, such as cancer cell lines, using optical and EM techniques. However, little is known about structural changes that may occur during disease in human tissue. There is a particular paucity of such information at high resolution as studies of the expression of clathrin in tissue have used conventional diffraction-limited optical microscopes.[15,16] Although diffraction-limited optical microscopes are commonly used in histologic investigations, their resolving capabilities are insufficient to visualize details below 200 nm in the lateral plane and cannot resolve structures at the protein level.[17] Although a novel set of super-resolution optical microscopy techniques can fulfill the resolution demands in such cases, the system complexity, high operating cost, lack of multimodality, and low-throughput imaging of these methods limit their wide adoption for histologic analysis. The application of SR-SIM to elucidate protein structure at nanometer scale in clinically useful human tissue samples *in situ*, as conducted here for clathrin, can further the understanding of both protein structure and mechanisms of disease in an accessible manner.

The advent of techniques such as stochastic optical reconstruction microscopy[18] and stimulated emission depletion microscopy[19] has allowed increased spatial resolution of clathrin pit structures; however, these studies have largely been restricted to cells grown in culture.[18–20] Here, multilabeled immunohistochemistry was applied in conjunction with super-resolution microscopy to present lattice SIM imaging where clathrin pit structures have been successfully resolved in clinical biopsy samples of human prostate. To our knowledge, this is the first report of clathrin pit structures being resolved successfully in human tissue.

The main goals of this study were threefold: i) to resolve clathrin pit structures and count their numbers in high- versus low-grade cancers; ii) to discern differences in size of individual clathrin pits in high- and low-grade cancers; and iii) to do so in numbers large enough that perhaps a biologically relevant difference may become apparent.

Understanding the spatial relationship of these three proteins (clathrin heavy chain, AP2, and EGFR) was also important in the context of this study as a means of verifying that clathrin pits had been resolved. Where previous studies resolved clathrin pit structures using techniques such as stochastic optical reconstruction microscopy or stimulated emission depletion microscopy,[21,22] this was not appropriate for imaging as the specimen must be grown or mounted on a coverslip. This type of processing is not possible for TAs as used here in an automated multiplex staining configuration, essential to conduct this investigation. In the case of stimulated emission depletion microscopy, there are limitations in use of commonly available fluorophores that can hamper multiple protein detection in samples. Lattice SIM offered an opportunity to multiplex multiple fluorophores relatively easily. It helped investigate the expression and structure of clathrin, the accessory protein AP2, and the cargo EGFR. Although at least two markers can be assessed simultaneously using immuno-EM (eg, using small and large immunogold particles, albeit with difficulty), no protein colocalization information can be gleaned from such an approach. While stochastic optical reconstruction microscopy allows multiplexing of more than two markers,[23] it is technically demanding and requires addition of special buffers to the tissue specimen. This is a particular challenge when investigating protein expression and structure in TAs with precious human samples and for achieving standardization with robust data acquisition using appropriate sample sizes. The SR-SIM approach is also not without its drawback.[24] These, for example, include reconstruction-induced,[25] parameter-dependent,[26] or structural mismatch artifacts. Even with these drawbacks, for which various mitigation strategies have been proposed,[24,26] the ability of lattice SIM to image large numbers of samples in clinical tissue samples without the requirement to add buffers to already stained samples (unlike stochastic optical reconstruction microscopy) and easy multiplexing of fluorophores (eg, compared with stimulated emission depletion microscopy) offer a unique advantage for the investigations of structural changes that may occur in human disease and one of the main reasons lattice SIM was chosen for this study.

The results shed light not only on the structure of clathrin in human tissue *in situ* but also reveal a biological and mechanistic relevance of these changes in cancer. These observations reveal a significant increase in the size of clathrin pits in high-grade cancer. Considering the critical role of CME in proliferative processes and overexpression of clathrin in cancer compared with normal prostate tissue, we proposed that a key role for CME may be in receptor recycling.[5] A key consequence of such an increase in the cargo capacity in cancer can be predicted to cause alteration in cell signaling and nutrient uptake. Alteration in cell signaling can include constitutive activation of EGF-EGFR pathway that can promote receptor recycling, rather than degradation and activation of downstream pathways that

favor carcinogenesis. Similar increase in other key signaling molecules, such as the Wnt pathway, may also occur. Increased cargo capacity also activates nutrient uptake and cellular resilience, promoting carcinogenesis through growth advantage, particularly in tumor microenvironment that is nutrient limited.[27,28] A further consequence of increased cargo capacity in CME is the disruption of cell junctions and integrin modulation, both processes that will lead to cancer progression and metastases.[29] The results presented here indicate that a key mechanism of achieving increased receptor recycling could be manifested by an increase in the clathrin pit size that may impact many different cellular processes, enhancing the fundamental understanding of carcinogenic mechanisms, and provide novel targets for cancer therapy.[29]

Author Contributions

A.A. conceived and designed the study; A.G., R.H., M.M., B.X., and A.A. performed experiments; A.G. and A.A. analyzed data; A.A. wrote the manuscript; and A.G., B.X., C.T., M.M., and R.H. reviewed the manuscript.

Disclosure Statement

None declared.

Supplemental Data

Supplemental material for this article can be found at *https://doi.org/10.1016/j.ajpath.2025.05.008*.

References

1. Brodsky FM: Clathrin structure characterized with monoclonal antibodies, I: analysis of multiple antigenic sites. J Cell Biol 1985, 101: 2047−2054
2. Smith CJ, Grigorieff N, Pearse BM: Clathrin coats at 21 A resolution: a cellular assembly designed to recycle multiple membrane receptors. EMBO J 1998, 17:4943−4953
3. Kaksonen M, Roux A: Mechanisms of clathrin-mediated endocytosis. Nat Rev Mol Cell Biol 2018, 19:313−326
4. Cocucci E, Aguet F, Boulant S, Kirchhausen T: The first five seconds in the life of a clathrin-coated pit. Cell 2012, 150:495−507
5. Xie B, Zuhair H, Henrique R, Millar M, Robson T, Thrasivoulou C, Dickens K, Pendjiky J, Muneer A, Patel H, Ahmed A: Opposite changes in the expression of clathrin and caveolin-1 in normal and cancerous human prostate tissue: putative clathrin-mediated recycling of EGFR. Histochem Cell Biol 2023, 159:489−500
6. Prakash K, Diederich B, Heintzmann R, Schermelleh L: Super-resolution microscopy: a brief history and new avenues. Philos Trans A Math Phys Eng Sci 2022, 380:20210110
7. Sauer M, Heilemann M: Single-molecule localization microscopy in eukaryotes. Chem Rev 2017, 117:7478−7509
8. Schermelleh L, Ferrand A, Huser T, Eggeling C, Sauer M, Biehlmaier O, Drummen GPC: Super-resolution microscopy demystified. Nat Cell Biol 2019, 21:72−84
9. Mockl L, Moerner WE: Super-resolution microscopy with single molecules in biology and beyond-essentials, current trends, and future challenges. J Am Chem Soc 2020, 142:17828−17844
10. Symes AJ, Eilertsen M, Millar M, Nariculam J, Freeman A, Notara M, Feneley MR, Patel HR, Masters JR, Ahmed A: Quantitative analysis of BTF3, HINT1, NDRG1 and ODC1 protein over-expression in human prostate cancer tissue. PLoS One 2013, 8:e84295
11. Arthurs C, Suarez-Bonnet A, Willis C, Xie B, Machulla N, Mair TS, Cao K, Millar M, Thrasivoulou C, Priestnall SL, Ahmed A: Equine penile squamous cell carcinoma: expression of biomarker proteins and EcPV2. Sci Rep 2020, 10:7863
12. Strohl FK CF: Frontiers in structured illumination microscopy. Optica 2016, 3:11
13. Schermelleh L, Heintzmann R, Leonhardt H: A guide to super-resolution fluorescence microscopy. J Cell Biol 2010, 190:165−175
14. Smith SM, Smith CJ: Capturing the mechanics of clathrin-mediated endocytosis. Curr Opin Struct Biol 2022, 75:102427
15. Xu Y, Yao Y, Yu L, Fung HL, Tang AHN, Ng IO, Wong MYM, Che CM, Yun JP, Cui Y, Yam JWP: Clathrin light chain A facilitates small extracellular vesicle uptake to promote hepatocellular carcinoma progression. Hepatol Int 2023, 17:1490−1499
16. Li G, Wang Y, Cao G, Ma Y, Li YX, Zhao Y, Shao X, Wang YL: Hypoxic stress disrupts HGF/Met signaling in human trophoblasts: implications for the pathogenesis of preeclampsia. J Biomed Sci 2022, 29:8
17. Villegas-Hernandez LE, Dubey V, Nystad M, Tinguely JC, Coucheron DA, Dullo FT, Priyadarshi A, Acuna S, Ahmad A, Mateos JM, Barmettler G, Ziegler U, Birgisdottir AB, Hovd AK, Fenton KA, Acharya G, Agarwal K, Ahluwalia BS: Chip-based multimodal super-resolution microscopy for histological investigations of cryopreserved tissue sections. Light Sci Appl 2022, 11:43
18. Huang Y, Ma T, Lau PK, Wang J, Zhao T, Du S, Loy MMT, Guo Y: Visualization of protein sorting at the trans-Golgi network and endosomes through super-resolution imaging. Front Cell Dev Biol 2019, 7:181
19. Arpino G, Somasundaram A, Shin W, Ge L, Villareal S, Chan CY, Ashery U, Shupliakov O, Taraska JW, Wu LG: Clathrin-mediated endocytosis cooperates with bulk endocytosis to generate vesicles. iScience 2022, 25:103809
20. Chen R, Tang X, Zhao Y, Shen Z, Zhang M, Shen Y, Li T, Chung CHY, Zhang L, Wang J, Cui B, Fei P, Guo Y, Du S, Yao S: Single-frame deep-learning super-resolution microscopy for intracellular dynamics imaging. Nat Commun 2023, 14:2854
21. Fernandez-Suarez M, Ting AY: Fluorescent probes for super-resolution imaging in living cells. Nat Rev Mol Cell Biol 2008, 9: 929−943
22. Jones SA, Shim SH, He J, Zhuang X: Fast, three-dimensional super-resolution imaging of live cells. Nat Methods 2011, 8:499−508
23. Klevanski M, Herrmannsdoerfer F, Sass S, Venkataramani V, Heilemann M, Kuner T: Automated highly multiplexed super-resolution imaging of protein nano-architecture in cells and tissues. Nat Commun 2020, 11:1552
24. Wang Z, Zhao T, Cai Y, Zhang J, Hao H, Liang Y, Wang S, Sun Y, Chen T, Bianco PR, Oh K, Lei M: Rapid, artifact-reduced, image reconstruction for super-resolution structured illumination microscopy. Innovation (Camb) 2023, 4:100425
25. Sahl SJ, Balzarotti F, Keller-Findeisen J, Leutenegger M, Westphal V, Egner A, Lavoie-Cardinal F, Chmyrov A, Grotjohann T, Jakobs S: Comment on "Extended-resolution structured illumination imaging of endocytic and cytoskeletal dynamics." Science 2016, 352:527
26. Perez V, Chang BJ, Stelzer EH: Optimal 2D-SIM reconstruction by two filtering steps with Richardson-Lucy deconvolution. Sci Rep 2016, 6:37149
27. Khan I, Steeg PS: Endocytosis: a pivotal pathway for regulating metastasis. Br J Cancer 2021, 124:66−75
28. Lopez-Hernandez T, Haucke V, Maritzen T: Endocytosis in the adaptation to cellular stress. Cell Stress 2020, 4:230−247
29. Banushi B, Joseph SR, Lum B, Lee JJ, Simpson F: Endocytosis in cancer and cancer therapy. Nat Rev Cancer 2023, 23:450−473